PERGAMON

Micron 30 (1999) 277–288

micron

www.elsevier.com/locate/micron

Applications of focused ion beam microscopy to materials science specimens

M.W. Phaneuf*

Fibics Incorporated, 568 Booth Street, Suite 224, Ottawa, Ontario, Canada K1A 0G1

Received 26 January 1999; received in revised form 26 January 1999; accepted 28 January 1999

Abstract

Focused ion beam (FIB) systems based on high-brightness gallium liquid-metal ion sources became commercially available in the late 1980s, although even today such instruments are relatively rare outside the somewhat enclosed world of semiconductor manufacturing. The use of FIB systems as precision sectioning tools down to a submicron scale and their ability to deposit metals and insulators on a micron scale is well documented. Recently, FIB systems have achieved spatial resolution rivaling that of the standard scanning electron microscope, giving them respectable capability as an imaging tool in addition to their sectioning and deposition capabilities. This improved resolution and novel FIB contrast mechanisms combined with the capability of FIB to produce in-situ stress-free bulk cross-sections and precision cross-sectional transmission electron microscopy specimens has recently attracted great interest among materials scientists. Examples of the use of FIB in materials science, both as a specimen preparation tool and as a microscope in its own right, are illustrated.

Keywords: Focused ion beam; Liquid-metal ion sources; FIB

1. Introduction

The technique of scanning a fine probe of charged particles and detecting the resulting signals to form a magnified image has been an integral part of materials science for more than thirty-five years, since the commercialization of the scanning electron microscope (SEM) (Pease and Nixon, 1965). The focused ion beam (FIB) microscope operates along the same principle as the SEM, in that a beam of charged particles is rastered across a specimen, and the resultant signal(s) at each raster position are plotted to form an image. However, in FIB the charged particle beam consists not of electrons, but rather (as the name implies) of ions, which are typically positively charged.

Different instruments exist which are capable of forming a beam of ions with micrometer or better spatial resolution, with secondary ion mass spectrometry (SIMS) systems being perhaps the most well known. In the past decade there have been a number of significant improvements in instruments based on liquid-metal ion sources (LMIS) employing gallium (Ga) ions as the primary beam, and recently commercially available Ga-LMIS instruments have achieved imaging resolution that, at 5 nm or better, rivals the standard SEM. These Ga-LMIS instruments, while merely members of the larger FIB family, have usurped somewhat the 'focused ion beam' moniker in the general literature, and henceforth in this paper the term 'FIB' will be used to describe such Ga-LMIS instruments, unless otherwise noted. These FIB systems have in common high-brightness ion sources capable of producing high current density beams suitable for in-situ sectioning, and frequently are also equipped with gas subsystems delivering a range of chemistries to permit ion-beam-assisted deposition and/or etching. Such systems are presently attracting growing interest in the field of materials science, and this article will attempt to illustrate why this is so.

The first documentation of ion emission from a liquid metal source came from the work of Krohn (1961), who was attempting to develop thrusters employing charged metal droplets for use in space flight. From this observation the LMIS was born, and while gas ion sources would replace LMIS as the technology of choice for space flight thrusters, LMIS would go on to find tremendous application in the semiconductor and materials analysis fields.

Although a number of LMIS systems world-wide were operated sporadically in the 1960s and 1970s, it was not until the 1980s that systematic work on the use of LMIS systems to perform scanning ion microscopy was undertaken. Prewett and Mair (1991) and Orloff (1993) have

* Tel.: + 1-613-860-0861.
E-mail address: mphaneuf@fibics.com (M.W. Phaneuf)

0968-4328/99/$ - see front matter
PII: S0968-4328(99)00012-8

documented the early evolution of FIB from both an instrument and application perspective, up to the point when the first commercial FIB instruments became widely available.

In the late 1980s, the versatility of these first commercially available FIB instruments, combined with the shrinking dimensions of very large scale integration (VLSI) integrated circuits, led to the adoption of FIB into the product cycle of semiconductor manufacturers. This resulted in a rapid increase in the number of applications of FIB, the complexity of FIB systems and the number of FIB systems sold worldwide. In 1986, the number of FIB fabrication systems totaled about 35 (Melngailis, 1987); in 1998, manufacturers of FIB systems estimate the number of such systems at 15–25 times that figure (Phaneuf, 1998). Subsequently, in the past 10 years, the volume of literature pertaining to FIB semiconductor applications has also increased, almost exponentially. It is outside the scope of this article to review and reference all of these applications, but as the semiconductor field has had such a great impact on the development of commercial FIB systems, the general categories along with a sampling of references to some early examples and/or overviews of these applications will be briefly discussed. Interested readers are encouraged to perform their own literature search, as a significant volume of work is now being published in this field every month.

Today's state-of-the-art FIB instruments are capable of many remarkable feats:

- imaging with 5 nm or better spatial resolution, using secondary electrons or secondary ions, exhibiting a number of novel contrast mechanisms;
- creating a precise cut or cross-section from a few tens of nanometres to a few hundreds of micrometres in size, with positional placement accuracy on the order of 20 nm (and in many cases tilting the specimen in situ for immediate imaging); and
- introducing several different gases into the vacuum chamber to either (i) deposit a range of materials up to 20 μm or more thick over areas ranging from the submicrometres to tens of thousands of square micrometres or (ii) selectively etch one material rapidly while barely affecting another.

2. FIB in the semiconductor industry

As mentioned above, applications in the semiconductor industry have been the driving force behind the commercialization of FIB systems; chronologically, first as direct device fabrication or lithography instruments (Cleaver and Ahmed, 1981; Cleaver et al., 1983; Gamo and Namba, 1991; Melngailis, 1993; Orloff, 1993) and semiconductor photomask repair tools (Heard et al., 1985; Nakagawa et al., 1988; Saitoh et al., 1988; Harriot, 1993), followed quickly by their application in circuit microsurgery to perform rapid prototyping (Melngailis et al., 1986; Lee and Morgan, 1991; Van Camp et al., 1996; Campbell et al., 1997; Benbrik et al., 1998) or circuit diagnostics and failure analysis (Kirk et al., 1987; Lee and Morgan, 1991; Mallard et al., 1998). In many cases these applications were made possible by the addition of gas chemistry into the FIB chamber that permit selective etching and metal or insulator deposition (Overwijk and van den Heuvel, 1993; Young et al., 1993; Casey et al., 1994; Hahn et al., 1995). Some overviews of these applications may be found in Melngailis (1987), Harriott (1991), Orloff (1993), Prewett (1993) and Young (1993). Although somewhat peripheral to the semiconductor field, related work has been undertaken in the applications of FIB to micromachining (Ishitani et al., 1990; Ishitani et al., 1991; Khamsehpour and Davies, 1993) and magnetic recording head trimming (McDermott, 1998).

Cross-sectional transmission electron microscopy (XTEM) specimen preparation of semiconductor devices using FIB systems was first demonstrated in the late 1980s (Kirk et al., 1989; Young et al., 1990; Basile et al., 1992) and is now a mainstay in the analysis of advanced semiconductor devices (Bender and Roussel, 1997; De Veirman and Weaver, 1999). As the basic techniques employed for semiconductor specimens are directly applicable to the production of materials science specimens for XTEM analysis, they are discussed here.

3. FIB in materials science

The use of FIB systems has been slowly making its way into the field of materials science, hampered not by limitations in the technique but rather by the relative scarcity of these instruments outside semiconductor fabrication facilities. It should be noted that a great deal of characterization work that has been performed in the semiconductor industry should rightly fall into the category of 'materials science', but for the purposes of this paper only non-semiconductor applications will be discussed. Further, the use of FIBs with high lateral resolution as part of SIMS analyses has been well covered elsewhere (see, for example, Benninghoven et al. (1987a), and the proceedings of the International Conferences on Secondary Ion Mass Spectrometry (Benninghoven et al., 1977, 1979, 1981, 1983, 1985, 1987b, 1989, 1991, 1993, 1995, 1997) as well as Levi-Setti et al. (1985, 1986)) and will not be reviewed here.

The use of FIB in materials science was initially weighted towards specimen preparation, but new instruments with high spatial resolution have made FIB imaging of materials specimens a rapidly growing field.

3.1. TEM specimen preparation

One FIB application developed for the semiconductor industry stands out as having the most significant impact thus far in the field of materials science: the use of FIB to prepare specimens for TEM. Early use of FIB techniques to

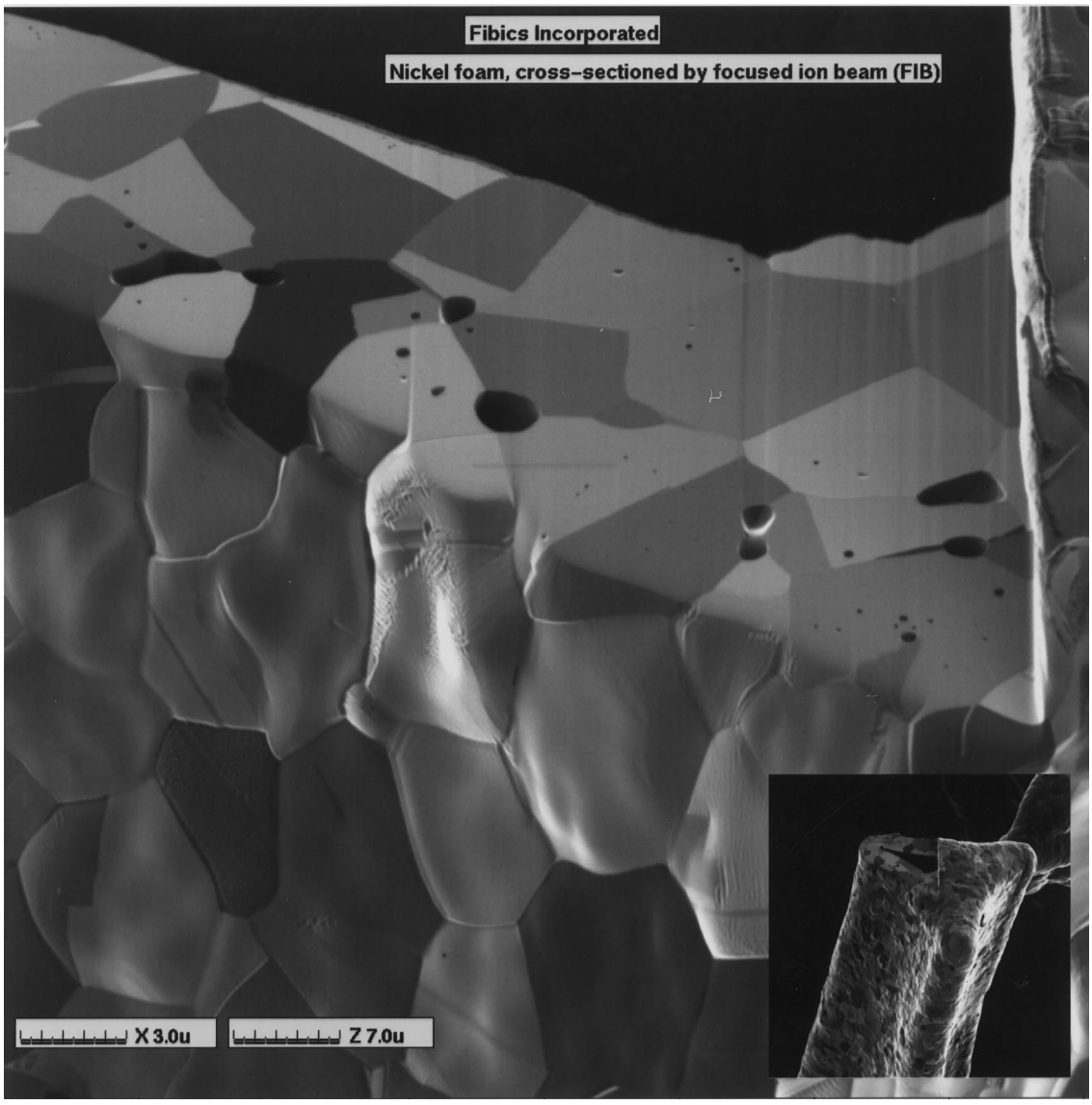

Fig. 1. FIB secondary electron mode image of a nickel foam 'strut' which forms a component of nickel-hydroxide-based batteries intended for automotive applications. One third of the tip of the strut has been sectioned in the FIB (inset) to expose internal detail. Both the sectioned and original surfaces have been imaged so as to illustrate the grain orientation contrast achievable in FIB secondary electron images, and the ability to reveal sub-micron voids and other fragile specimen features without the stress and potential damage involved in mechanical sectioning.

perform precise cross-sectioning of semiconductor devices can be found in Kirk et al. (1989), Park (1990), Young et al. (1990) and Basile et al. (1992) who employed the 'bar-H' technique whereby an electron-transparent membrane is produced by FIB milling of back-to-back sections into a mechanically thinned bar mounted on a modified aperture TEM grid. Overwijk et al. (1993) and Giannuzzi et al. (1998, 1999) employed the 'lift-out' technique, whereby a similar membrane is produced in a bulk sample, then cut free using the FIB and removed for stand-alone examination in the TEM. More details regarding both the 'lift out' and 'bar H' techniques may be found in the articles of Giannuzzi et al., and De Veirman and Weaver, which can be found in this issue.

Some of the first non-semiconductor materials to be examined using FIB specimen preparation for TEM were micrometre-scale particles of nickel powder and magnesium–zinc alloy (Kitano et al., 1995a,b), such sized particles being extremely difficult to prepare by conventional means. In both these work, the metal powders were thinned sufficiently to provide large areas suitable for high-resolution electron microscopy (HREM).

Galvannealed steel sheet composed of several micrometres of various iron–zinc intermetallic phases coating a steel substrate is another material difficult to prepare by conventional means, due to the vastly different sputter rates exhibited by the intermetallics under conventional argon-ion milling. Specimen preparation by FIB was applied successfully by Saka et al. (1995) and Phaneuf et al. (1997), who also demonstrated the ability of FIB

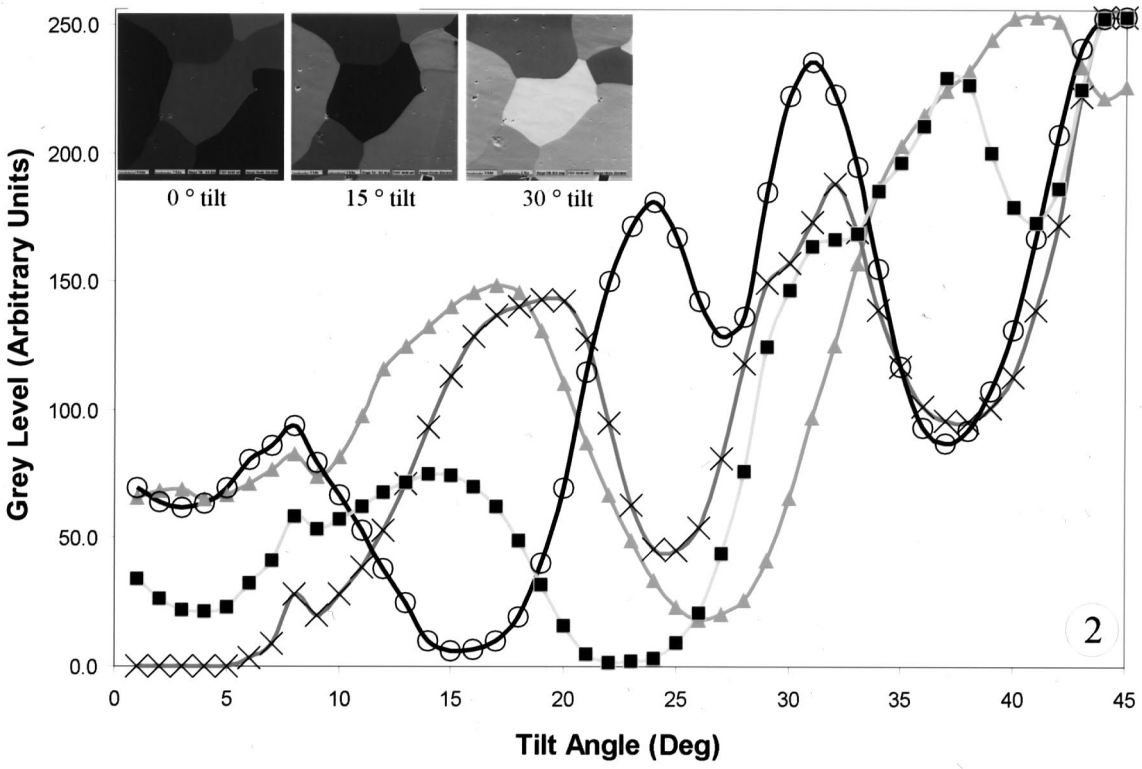

Fig. 2. FIB secondary electron mode orientation contrast of a fully annealed, nominally pure polycrystalline aluminum specimen changes the intensity (grey level) of each grain as a function of deviation from normal incidence as the specimen is tilted with respect to the gallium beam. The same region is imaged (inset) at angles of 0, 15, and 30° tilt (foreshortening due to tilt angle is evident). The change in intensity (in arbitrary 'grey level' units) is plotted as a function of tilt angle in 1° increments. Dark grains (low intensity) represent significant channeling of the primary ions. The angular width of channeling 'troughs' and the angular distance between troughs can be used to calculate the relative orientation of different grains.

secondary electron imaging (SEI) to elucidate the microstructure of the coating.

The sub-micrometre positional accuracy of the FIB TEM sample preparation technique was employed by Muroga and Saka (1995) to produce bar-H style specimens to observe the defect structures produced by rolling-contact fatigue in steels, and by Saka and Abe, (1997a,b) to examine crack tips produced by Vickers indentation into dislocation-free single crystals of silicon. In the latter works, general features of the microstructure near an indentation were observed before and during in-situ heating experiments in the TEM.

Although the examples given here used the bar-H technique to prepare specimens for FIB, the lift-out technique has also been applied successfully to a number of materials science problems including various forms of the iron–zinc system to produce TEM specimens with little or no prior sample preparation (Giannuzzi et al., 1998), at the expense of slightly thicker (on average) samples than can be produced by the bar-H method, or samples that are deliberately 'wedged' in thickness laterally across the electron transparent thin area.

By 1998, TEM specimens of many different materials had been successfully prepared by FIB in a number of locations world-wide. In our laboratory alone we have prepared over 200 TEM specimens of more than three dozen materials, and we are relatively newcomers to the FIB field, having only received our Micrion 2500 FIB system in mid-1997.

3.2. In-situ sectioning and imaging with FIB contrast mechanisms

As the imaging resolution of FIB instruments improved to the level where FIB can compete with conventional SEM in the latter half of the 1990s, applications combining in-situ FIB sectioning with FIB imaging have attracted significant attention in the materials science community. The benefits of this combination are clearly demonstrated in Fig. 1, which shows a nickel-foam 'strut' which forms a component of nickel hydroxide based batteries intended for automotive applications. Here the tip of the strut has been sectioned in the FIB (inset), and both the sectioned and original surfaces have been imaged so as to illustrate the grain-orientation contrast achievable in FIB secondary electron images, and also the ability to reveal sub-micrometre voids and other fragile specimen features without the stress and potential damage involved in mechanical sectioning. Ishitani et al. (1995) illustrated the benefits of stress-free sectioning by cross-sectioning portions of human hair and the compound eye of a housefly, although fine scale FIB

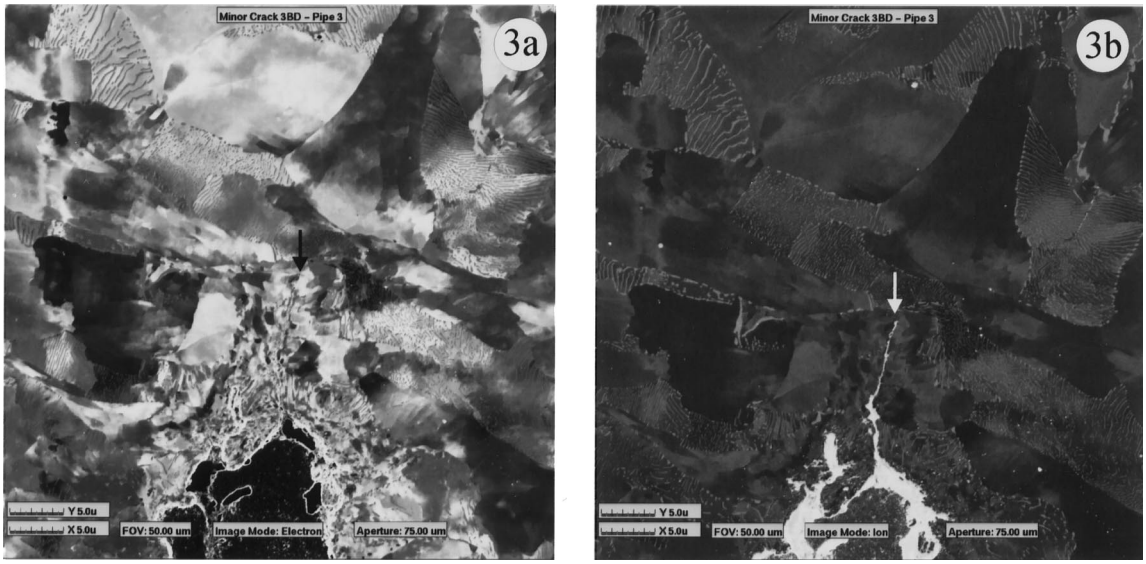

Fig. 3. A metallographically polished specimen of a steel pressure vessel containing a corroded crack is imaged in secondary electron mode (3a) and secondary ion mode (3b). In ion mode, the increased yield of secondary ions from the oxygen present in the corrosion product filling the crack tip delineates the crack very effectively. In our Micrion 2500 FIB system, the same 'D' shaped, coaxially mounted microchannel plate detector is used to detect both types of secondary particle, biased at + 400 V in secondary electron mode and at − 1500 V in secondary ion mode. Changing the bias when changing from one imaging mode to the other results in a change in electric field gradient causing the image in 3(b) to shift vertically down the page with respect to 3(a). Arrows mark the crack tip in each image.

induced damage is evident in the form of a general 'blurring' of the cross-sectioned face in the micrographs of their specimens. FIB induced damage can be a serious concern, particularly in 'soft' systems prone to ion induced surface damage. FIB deposition of a protective metal layer prior to sectioning, combined with care and experimentation with regard to beam parameters, are frequently required to minimize this type of artifact to an acceptable level.

Specimen preparation by FIB milling need not be limited to imaging applications. Davis (1997) describes the use of FIB micromachining to produce extremely sharp pre-cracks in microcharpy impact test specimens, and we have used similar techniques in our laboratory to produce specimens for microtensile testing. Similar studies are reported by Presser and Hilton (1997) and Young (1997).

FIB imaging is performed with either secondary ions or secondary electrons ejected by interaction of the primary beam with the sample surface. These secondary particles possess energies of only a few electron volts, and are readily detected on an 'all or nothing' basis using a collector such as a microchannel plate biased positively at a few hundred volts for secondary electron detection or negatively by a few thousand volts for positive secondary ion collection. In the Micrion FIB system, the detector is mounted coaxially at the base of the FIB column and provides a large solid angle for secondary particle detection.

Contrast mechanisms in FIB images have been discussed previously (Prewett and Mair, 1991; Olson et al., 1992; Ishitani and Tsuboi, 1996) and for materials science specimens they fall largely into the categories of crystallographic orientation (channeling) contrast, material contrast and topographic contrast. Several contrast mechanisms interact simultaneously in typical FIB images and as in most beam instruments suppressing or enhancing one particular mechanism can enhance details in the image.

Orientation contrast is perhaps the most striking feature of FIB microscopy of metallic specimens, and arises from channeling of the incident ions between lattice planes of the specimen. Depth of penetration of the channeled incident ion varies with the relative angle between the ion beam and the lattice plane and the interplanar spacing of the lattice. Although channeling contrast is exhibited in both the secondary electron and secondary ion images, secondary electron yield is significantly greater than that of secondary ions for most materials, and is less sensitive to changes in chemistry. Early examples of this effect were published by Levi-Setti et al. (1983) and Franklin et al. (1988). Fig. 2 illustrates this phenomenon in a nominally pure aluminum alloy, where grain intensity is plotted versus deviation from normal incidence as the specimen is tilted through 45° relative to the ion beam. Each line in the figure represents the change in intensity of a discrete grain. Wang et al. (1998) used FIB orientation contrast to image grains of Al–Li–Cu alloys, despite their non-periodic quasicrystalline structure.

Material contrast arises from differences in the yield of secondary particles as a function of specimen chemistry. Although this effect can be significant in FIB secondary electron images, it is most readily observed in FIB secondary ion images where it is frequently the dominant contrast effect. Secondary ion yields from gallium beams can increase by up to three orders of magnitude for metallic species in the presence of oxygen, making material contrast

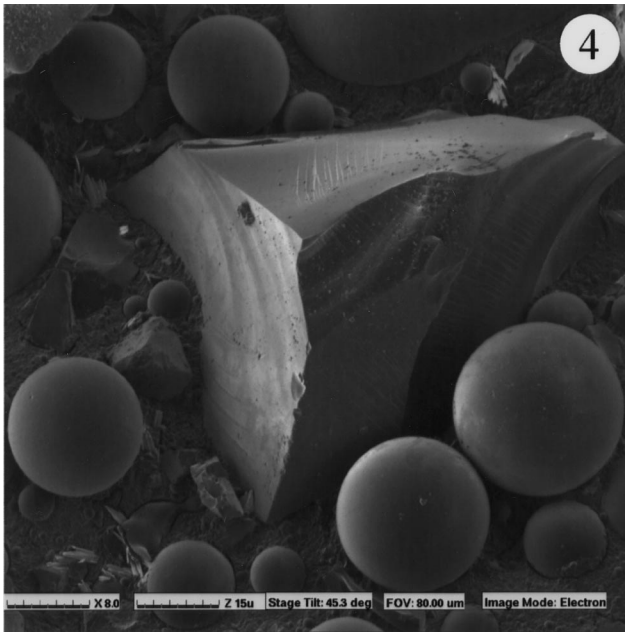

Fig. 4. Topographic contrast imaging in secondary electron mode. Glass-based particulate in the form of small spheres and larger angular fragments is used in the encapsulation of semiconductor devices. Here, the encapsulant plastic has been removed by acid etching external to the FIB. The shape of both spherical and angular particles is readily discernible due to the familiar nature of topographic contrast.

a valuable technique for studies involving corrosion or grain boundary oxidation of metals. Fig. 3 shows the value of material contrast in such a study; a corroded crack in a steel pressure vessel is readily apparent, even at low magnifications (large fields of view (FOV)), when imaging in ion mode due to the greatly enhanced secondary ion yield from the oxidized corrosion product in the crack tip. For comparison, the same crack region is shown in both secondary ion and secondary electron images (Fig. 3a and b, respectively).

Topographic contrast is familiar to anyone who has seen an SEM image of an irregular object, and even those unfamiliar with images from beam instruments readily interpret topographic contrast images due to their similarity to optical images viewed with directed illumination. In general, topographic contrast in FIB (Prewett and Mair, 1991; Olson et al., 1992) has previously been explained in a similar manner to topographic contrast in SEM, in terms of differences in signal (secondary electron and ion production) as a function of the angle of incidence of the primary beam relative to specimen surface normal as the local inclination of the specimen surface varies. This effect is then convolved with detector geometry to produce an image with many features familiar to the casual observer. Fig. 4 illustrates topographic-contrast imaging of glass-based particulate in the form of small spheres and larger angular fragments which are used in the encapsulation of semiconductor devices. These particles are generally non-crystalline and in Fig. 4 are exposed by removing the bulk of the plastic encapsulant material with fuming nitric acid prior to entering the FIB. It should be noted that topographic contrast is frequently overwhelmed by channeling contrast in certain material systems and geometries. Fig. 1 illustrates a combination of topographic and orientation contrast. On the FIB sectioned top surface of the nickel strut there is essentially no topography, and orientation channeling contrast dominates. On the side of the nickel strut no sectioning has been performed; in addition to the orientation contrast the effect of the original topography, plus that which has evolved during repeated FIB imaging prior to sectioning, is visible.

Prewett and Mair (1991) point out there has been little objective analysis of topographic contrast compared to the effort spent analyzing the other dominant contrast mechanisms in FIB images. Further study of topographic contrast is required to resolve differences in topographic contrast between secondary-ion and secondary-electron imaging in the FIB, and differences between secondary electron imaging in the FIB and in the SEM.

4. Examples of FIB applications in materials science

As mentioned previously, the high spatial resolution available in the latest generation of FIB microscopes, combined with FIB's capability for in-situ 'stress-free' sectioning, makes the FIB a very attractive instrument for materials characterization. In the section that follows, a number of materials science applications that have been undertaken in our laboratory are illustrated.

At this point, a note on interpretation of FIB images from a spatial perspective is in order. Unlike most SEM images, FIB images are typically shown with two scale bars. One scale bar is the 'X scale', referring to the horizontal direction (relative to the stage's tilt axis) across the image, while the other (either 'Y scale' or 'Z scale') is calibrated for measurement 'down' the image's vertical axis as a function of stage tilt. On our Micrion 2500 system, the software that produces the calibrated scale markers assumes that at any stage tilt angle greater than 20°, the user is most interested in an accurate measurement down the cross-sectional ('Z' axis) face, and shows the appropriate 'Z scale' bar. Thus, a FIB image taken at a 45° tilt of a FIB's cross-section will have two scale bars, an 'X scale' for horizontal measurements and a 'Z scale' for measurement down the cross-section. At stage tilt angles less than 20°, the software assumes measurements are desired for 'X' and 'Y' in plan view, and produces 'X scale' and 'Y scale' bars accordingly. Naturally, if the stage tilt is 0°, the 'X' and 'Y' scale bars are of equal length, but at non-zero stage tilt foreshortening as a function of tilt angle must be included in any interpretation of the shape of a given feature.

4.1. FIB orientation channeling contrast imaging of the microstructure of a polymer coated aluminum beverage can

The common aluminum beverage can is a highly

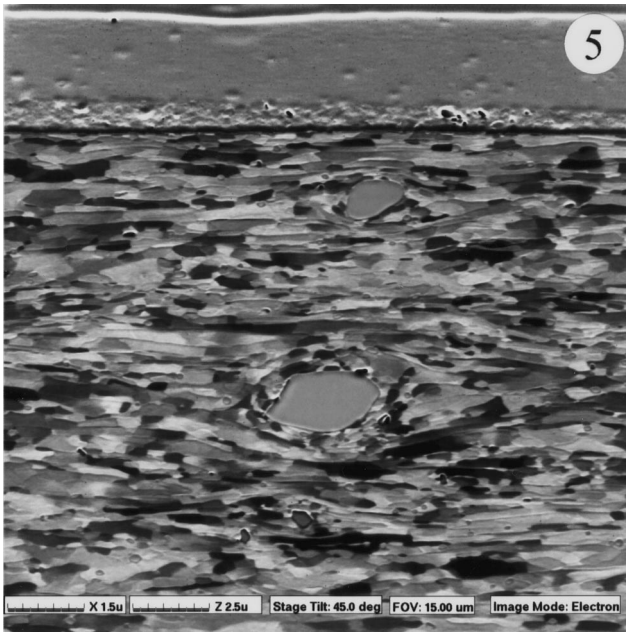

Fig. 5. FIB secondary electron image of a FIB cross-section into an aluminum beverage can. The polymer label on top of the aluminum is clearly visible, and manganese silicate particles (as determined by EDX in a SEM) can be seen amid the aluminum grain orientation contrast.

engineered structure. FIB cross-sectioning and imaging reveals the elongated grain structure of the aluminum alloy, the polymer label on the surface of the aluminum and manganese inclusions (Fig. 5) whose chemistry was determined by energy dispersive X-ray spectroscopy during subsequent SEM analysis. 'Dual beam' FIB instruments, consisting of both a FIB column and a SEM column with an EDX detector, exist and permit sectioning, imaging and chemical analysis all in the same chamber.

4.2. FIB stress-free sectioning to reveal failure mechanisms of titanium diboride reinforced zinc–aluminum metal–matrix composites after fracture toughness testing

A FIB cross-section was prepared from a sample of 23.3 (vol.%) TiB_2-particle-reinforced ZA-8 (zinc–8 wt.% aluminum foundry alloy) metal–matrix composite (Dionne, 1999). This material is composed of hard particles in a soft matrix and it is very difficult to polish using metallographic techniques without introducing artefacts such as broken particles, pull-outs and smearing. For examination in the FIB instrument, a fracture toughness sample of the composite was cut perpendicularly to the fracture surface using a low-speed diamond saw. FIB polishing was used to create a box 100 μm wide by 100 μm high by 40 μm deep on the cut surface just below the fracture plane. The removal by FIB milling of about 40 μm of material from the cut surface was sufficient to eliminate the damage produced by the diamond saw.

Fig. 6 shows a typical secondary electron FIB image obtained from the polished cross-section. Two TiB_2 particles are embedded in the ZA-8 matrix which is composed of the zinc η phase (light contrast) and lamellar Al-rich α phase (darker contrast) in accordance with the Zn–Al phase diagram. Secondary cracks resulting from the fracture toughness test are located in the matrix, in one particle and along part of the particle–matrix interface. However, the particle and interface cracks have not extended into the matrix, showing that matrix cracking has occurred independently of particle failure. Based upon these observations, we can conclude that matrix cracking is not initiated by particle failure in this composite system. In addition, the grain contrast inherent to the FIB imaging process reveals the presence of several grains and small pores in the large TiB_2 particle on Fig. 6. These observations invalidate a common assumption of many models of metal–matrix composite properties, in which the reinforcement particles are supposed to be perfect single crystals.

4.2.1. FIB secondary electron material contrast exposes entrainment of reaction products during the production of magnesium–silicon carbide metal matrix composites

A magnesium-alloy metal–matrix composite material reinforced with silicon carbide (SiC) particles was manufactured by squeeze casting (Lo et al., 1996). During the initial metal infiltration, magnesium reacts with silicon dioxide present on the SiC particle surface to form magnesium oxide (MgO). Subsequent processing can delaminate this thin reaction product layer, allowing it to become entrained in the magnesium matrix where a combination of its plate-like geometry and the inherent brittleness of MgO can act as an initiating site for crack formation under the influence of mechanical stress. FIB sectioning and imaging (Fig. 7) reveal these fine details through a combination of topographic and chemical contrast.

4.3. FIB precision sectioning and orientation contrast enhances monitoring of stress-corrosion cracking specimens during long-term corrosion studies

As part of an on-going study, cracks developing on samples of a X-65 grade pipeline steel cyclically loaded in a dilute simulated ground water solution with near-neutral pH were imaged in plan view, precision cross-sectioned at different locations along the length of a given crack, and then tilted to permit viewing the cross-sectioned surface (Fig. 8). Information regarding the grain structures around the crack tip, and accurate measurement of the crack length and depth were obtained without disrupting neighboring cracks. The granular crack path and other microstructural features associated with crack development were clearly illustrated, and it was possible to return the specimen to the ground water solution to continue the test. Iteration of this process provided crack aspect ratio and evolution data on the same specimen in an efficient manner (Wang et al., 1999).

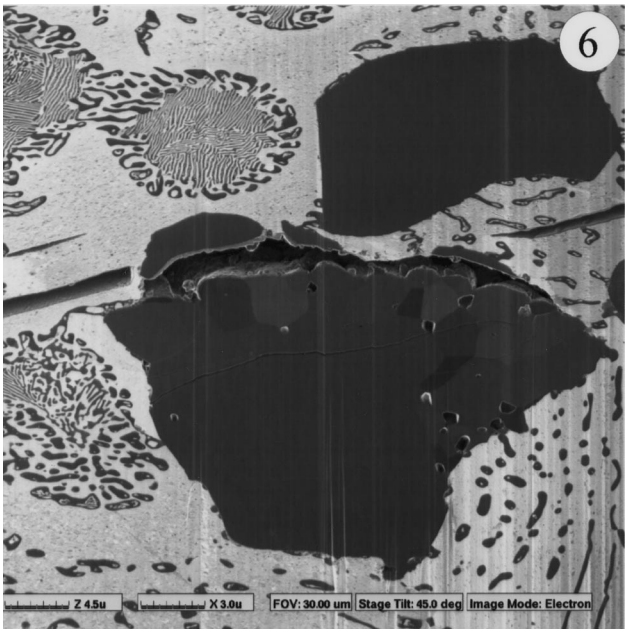

Fig. 6. FIB secondary electron image obtained from a FIB polished cross-section in a Zn–Al alloy reinforced with TiB_2. Two TiB_2 particles are visible in the alloy matrix which is composed of the zinc η phase (light contrast) and lamellar Al-rich α phase (darker contrast) in accordance with the Zn–Al phase diagram. Secondary cracks resulting from the fracture toughness test are located in the matrix, in one particle and along part of the particle–matrix interface. However, the particle and interface cracks have not extended into the matrix, showing that matrix cracking has occurred independently of particle failure. Based upon these observations, we can conclude that matrix cracking is not initiated by particle failure in this composite system. In addition, orientation contrast reveals the presence of several grains and small pores in the large TiB_2 particle. These observations invalidate a common assumption of many models of metal–matrix composite properties, in which the reinforcement particles are supposed to be perfect single crystals.

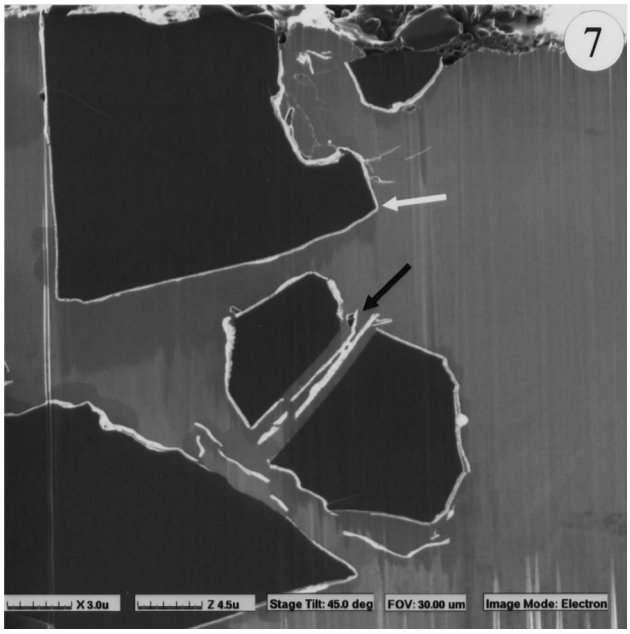

Fig. 7. FIB sectioning of a SiC reinforced Mg alloy. A reaction product of MgO forms between the SiC particles and the Mg alloy. In some cases this reaction product remains adhered to the SiC surface (white arrow), while in others it detaches (black arrow) and becomes entrained in the matrix (black arrow). Its plate-like geometry and the inherent brittleness of MgO can act as an initiating site for crack formation under the influence of mechanical stress. FIB imaging reveals these fine details through a combination of topographic and chemical contrast.

4.4. Analysis of nickel hydroxide particles after numerous charge–discharge cycles

The failure mechanism whereby a nickel-hydroxide-based battery electrode loses its ability to retain charge is still under debate. In order to examine changes in the morphology of nickel hydroxide particles in these batteries, a battery electrode that had reached the end of its useful lifetime (more than 6000 charge–discharge cycles) was sectioned in a stress-free manner without any mechanical pre-preparation other than critical-point drying (Fig. 9, inset). After tilting to view the cross-sectioned face, FIB topographic contrast revealed the ‘pulverized’ look of the nickel hydroxide particles which had been composed of radially oriented plates at the beginning of the experiment. Foreshortening due to stage tilt has given these essentially spherical particles an elliptical appearance.

4.5. FIB XTEM specimen preparation of surface oxide on Zr–2.5%Nb CANDU reactor pressure tube material

Precision, ‘stress-free’ FIB sectioning can be used to

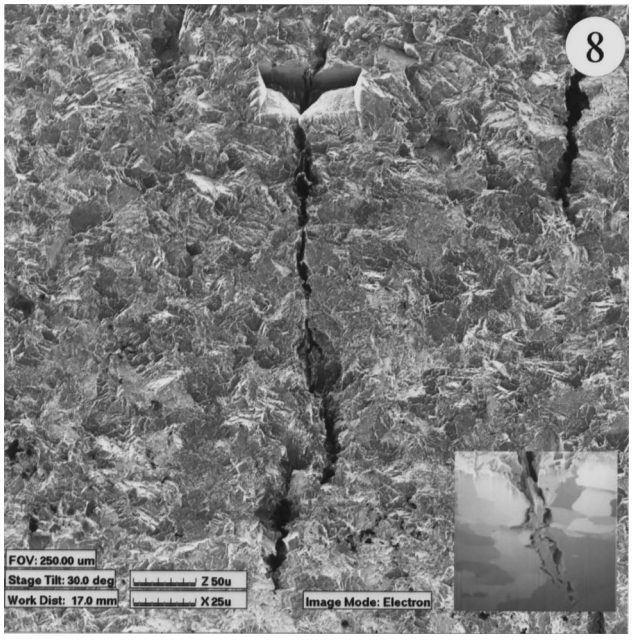

Fig. 8. A FIB cross-section (top centre) of a stress-corrosion crack in an X-65 grade pipeline steel. The precision section does not substantially effect the neighboring cracks. Inset: FIB image of the sectioned face reveals intergranular corrosion and permits measurement of the depth of the crack.

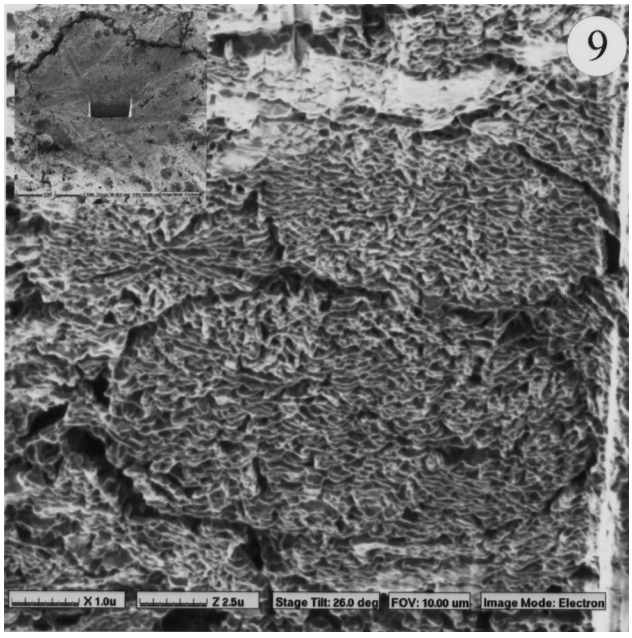

Fig. 9. Nickel hydroxide particles in an end-of-lifetime battery electrode are sectioned and imaged in the FIB, revealing the fine structure nickel hydroxide particles made up of of 'pulverized' platelets. Fine details of mechanically fragile specimens are preserved by stress-free FIB sectioning.

prepare EELS thin TEM cross-sections of 'challenging' specimens, such as this surface oxide grown in 300°C water on Zr-2.5Nb CANDU reactor pressure-tube material (Fig. 10). In this specimen, cracks running horizontally through the oxide film have been preserved in the TEM section. In many cases a protective layer of FIB-deposited

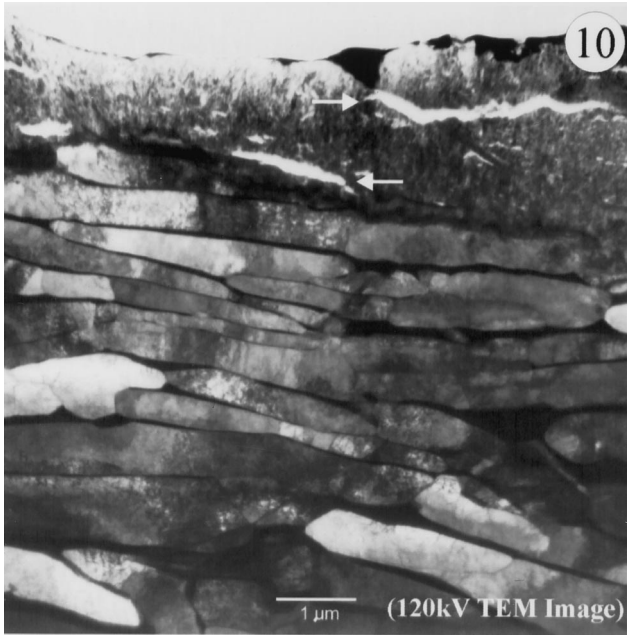

Fig. 10. Precision, 'stress-free' FIB sectioning can be used to prepare EELS thin TEM cross-sections of 'challenging' specimens, such as this surface oxide grown in 300°C water on Zr–2.5Nb CANDU reactor pressure tube material. Horizontal 'cracks' in the surface oxide are indicated (arrows).

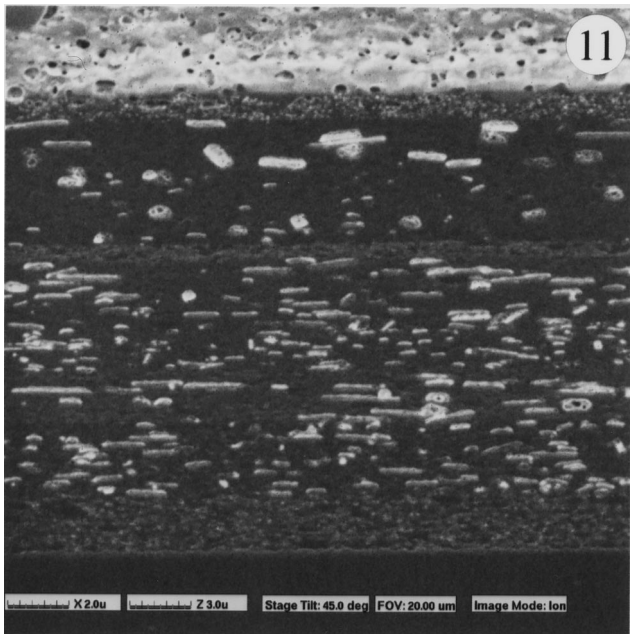

Fig. 11. FIB secondary ion image of a FIB cross-section through the surface of a 200 ASA color photographic film. The porous surface layer, and layers of 'colour grains' lying primarily in the plane of the film, separated by 'filter layers' are clearly distinguishable.

metal such as tungsten or platinum is deposited prior to sectioning to preserve the surface structure and reduce streaking caused when milling through regions of varying density. The remains of a protective tungsten layer (dark contrast) are just visible above the oxide film. Preferably, a thicker layer would be used to prevent any loss of surface material.

4.6. Rapid FIB cross-sectioning and imaging through 200 ASA colour photographic film

Cross-sectional examination of thin layers on somewhat flimsy substrates can pose a daunting specimen preparation task. Although such samples frequently lend themselves to ultramicrotomy, the tearing that can be associated with this technique introduces undesirable artifacts. Fig. 11 shows a FIB cross-sectional image of the active surface layers of a 200 ASA colour photographic film. Although some evidence of fine scale sputter damage is evident, both the silver based 'colour grains' at various levels in the film and the selective light filtering layers between these levels are clearly resolved. Specimen pre-preparation consisted of cutting a millimeter wide slice from the leader of a film reel. The time from the film reel to the digital image of the cross-section was below 20 min.

4.7. FIB secondary ion chemical contrast as an aid to qualitative determination of the carburization of heat resistant alloys

The most common FIB instruments do not possess any means of chemical analysis such as mass spectrometry,

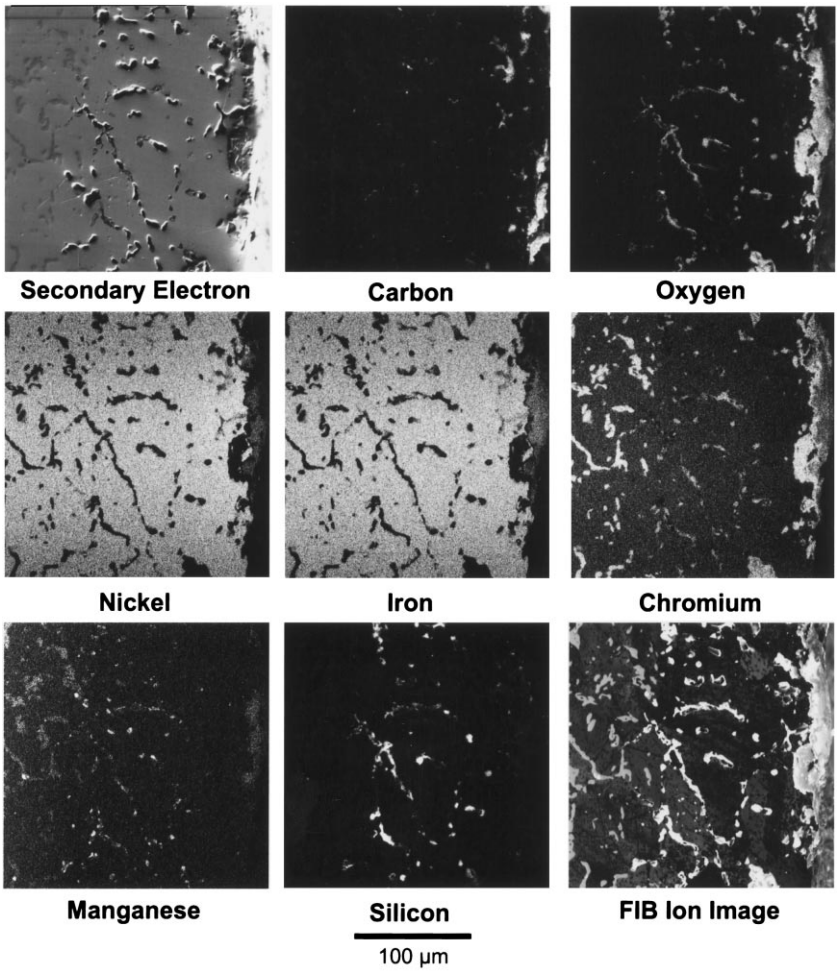

Fig. 12. Analysis of a carburized Fe–Ni–Cr heat resistant alloy by X-ray mapping of seven elements in the electronprobe microanalyzer is compared to the information available in a single FIB secondary ion image. As secondary ion production is heavily influenced by matrix chemistry, a great deal of information is available in the FIB ion image. Much like learning optical metallography, given sufficient initial references (such as a few somewhat time consuming X-ray maps), one can learn to recognize the different phases present in such a material from an ion image that can be acquired in a matter of a few seconds.

although at least two manufacturers of commercial instruments offer this as an optional add-on, and dedicated SIMS instruments are now relatively commonplace. Despite the lack of true chemical analysis, as Fig. 12 illustrates secondary ion chemical contrast can be used to make qualitative judgements on the chemical species present in certain samples, such as the near-surface region of a heat-resistant alloy Fe–Ni–Cr alloy after pack-carburization testing (Milner and Phaneuf, 1998).

Fig. 12 compares the results of X-ray mapping of seven elements in the electronprobe microanalyzer to the information available in a single FIB secondary ion image. Both the EPMA and FIB images were acquired from the same region of a metallographically polished specimen. As secondary ion production is heavily influenced by matrix chemistry, a great deal of information is available in the FIB ion image. Much like learning optical metallography, given sufficient references (such as, a few somewhat time consuming X-ray maps), one can learn to recognize the different phases present in such a material from an ion image that can be acquired in a matter of a few seconds.

5. Concluding remarks

A great deal of interest is now being demonstrated in the application of FIB systems to materials science problems. FIB was virtually unknown in the materials science community half a decade ago (outside its use in the field of SIMS chemical analyses). Now, conference presentations and journal articles that mention the use of FIB in materials science applications, while not yet ‘common place’, are certainly increasing in number at a tremendous rate. Nevertheless, a great deal of fundamental research remains to be performed with regard to a more detailed understanding and harnessing of beam–specimen interactions. Initially driven by the semiconductor industry, commercial manufacturers are now turning their attention to materials scientists to elicit feed-back regarding future instrument developments aimed

at materials analysis. In the future, one can expect commercially available hot, cold and tensile stages, dual beam instruments combining the benefits of FIB with electron-induced chemical analysis and orientation imaging or electron backscatter pattern (EBSP) crystallographic analysis and higher current columns capable of faster bulk sectioning of dense materials to produce cross-sections that range up to hundreds of micrometers in length and depth. Also, present research into the use of gas field ion sources to replace liquid-metal ion sources holds the promise of nanometre-scale beams of ions ranging from hydrogen to oxygen to xenon, and with that greatly enhanced SIMS capability compared to that presently available with gallium beams. These sources also open up the possibility of RBS-like analysis and chemical analysis via ion-induced X-ray emission. The future of FIB in materials analysis is bright, and the present holds many opportunities for both research and application driven usage of this technology.

References

Basile, D.P., Boylan, R., Baker, B., Hayes, K., Soza, D., 1992. FIBX-TEM—Focused ion beam milling for TEM sample preparation. In: Anderson, R., Tracy, R., Bravman, B. (Eds.). Materials Research Society Symposium Proceedings, 254. MRS, Pittsburgh, pp. 23–41.

Benbrik, J., Rolland, G., Perdu, P., Benteo, B., Casari, M., Desplats, R., Labat, N., Touboul, A., Danto, Y., 1998. Focused ion beam irradiation induced damages on CMOS and bipolar technologies. Proceedings of the Twentyfourth International Symposium for Testing and Failure Analysis, ISTFA '98, pp. 49–55.

Bender, H., Roussel, P., 1997. Cross-sectional transmission electron microscopy and focused ion beam study of advanced silicon devices. In: Inst. Phys. Conf. Ser. Proc. Microscopy of Semiconducting Materials X. (In press).

Benninghoven, A., Rudenauer, F.G., Werner, H.W., 1987. Secondary Ion Mass Spectrometry: Basic Concepts, Instrumental Aspects, Applications and Trends. Wiley, New York.

Benninghoven et al. (Eds.), Proceedings of the International Conference(s) on Secondary Ion Mass Spectrometry (SIMS I through IV, 1977 1979, 1981, 1983, Springer, Berlin), (SIMS V through XI, 1985, 1987b, 1989, 1991, 1993, 1995, 1997, Wiley, New York).

Campbell, A., Perderson, K.A., Fleetwood, D.M., 1997. Effects of focused ion beam irradiation on MOS transistors. Proceedings Thirtyfifth Annual International Reliability Physics Symposium, IRPS '97, pp. 72–81.

Casey, J.D., Doyle, A.F., Lee, R.G., Stewart, D.K., 1994. Gas-assisted etching with focused ion beam technology. Microelectronic Engng 24, 43–50.

Cleaver, J.R.A., Ahmed, H., 1981. A 100 kV ion probe microfabrication system with a tetrode gun. J. Vac. Sci. Technol. 19 (4), 1145–1148.

Cleaver, J.R.A., Heard, P.J., Ahmed, H., 1983. Scanning ion beam lithography with a magnetic ion species filter. In: Ahmed, H., Cleaver, J.R.A., Jones, G.A.C. (Eds.). Microcircuit Engineering, 83. Academic Press, London, pp. 135–142.

Davis, R.B., 1997. Preparation of samples for mechanical property testing using the FIB workstation. Microstr. Sci. 25, 511–515.

Dionne, S., 1999. Influence of titanium diboride reinforcements on the microstructure, mechanical properties and fracture behaviour of cast zinc–aluminum composites, Ph.D. Thesis Dissertation, Université Laval, Province du Québec, Canada.

Franklin, R.E., Kirk, E.C.G., Cleaver, J.R.A., Ahmed, H., 1988. Channelling ion image contrast and sputtering in gold specimens observed in a high-resolution scanning ion microscope. J. Mat. Sci. Lett. 7, 39–41.

Gamo, K., Namba, S., 1991. Recent advance of focused ion beam technology in maskless deposition and patterning. Nucl. Instrum. Methods B. 59/60, 190–196.

Giannuzzi, L.A., Drown, J.L., Brown, S.R., Irwin, R.B., Stevie, R., 1998. Applications of the FIB lift-out technique for TEM specimen preparation. Microsc. Res. Tech. 41, 285–290.

Hahn, L.L., Abramo, M., Doyle, A., Moszkowicz, L., Stewart, D., 1995. Focused-ion-beam-induced insulator deposition for chip circuit modification. Thin Solid Films 270, 422–425.

Harriott, L.R., 1991. The technology of finely focused ion beams. Nucl. Instrum. Methods B 55, 802–810.

Harriot, L.R., 1993. Focused Ion beam XeF2 etching of materials for phase-shift masks. J.Vac. Sci. Technol. B 11 (6), 2200–2203.

Heard, P.J., Cleaver, J.R.A., Ahmed, H., 1985. Application of a focused ion beam system to defect repair of VLSI masks. J.Vac. Sci. Technol. B 3 (1), 87–90.

Ishitani, T., Hirose, H., Tsuboi, H., 1995. Focused-ion-beam digging of biological specimens. J. Electron Microsc. 44, 110–114.

Ishitani, T., Tsuboi, H., 1996. Objective comparison of scanning ion and scanning electron microscope images. Scanning 19, 489–497.

Ishitani, T., Ohnishi, T., Kawanami, Y., 1990. Micromaching and Device Transplantation Using Focused Ion Beam. Jpn. J. App. Phys. 29 (10), 2283–2287.

Ishitani, T., Ohnishi, T., Madokor, Y., Kawanami, Y., 1991. Focused-ion-beam 'cutter' and 'attacher' for micromachining and device transplantation. J. Vac. Sci. Technol. B 9 (5), 2633–2637.

Khamsehpour, B., Davies, S.T., 1993. Drilling of fine apertures in thin metallic foils using a focused ion beam. Vacuum 44 (3/4), 361–365.

Kirk, E.C.G., Cleaver, J.R.A., Ahmed, J., 1987. In situ microsectioning and imaging of semiconductor devices using a scanning ion microscope, Inst. Phys. Conf. No.87, Section 11, pp. 691–693.

Kirk, E.C.G., Williams, D.A., Ahmed, H., 1989. Cross-sectional transmission electron microscopy of precisely selected regions from semiconductor devices. Inst. Phys. Ser. 100, 501–506.

Kitano, Y., Fujikawa, Y., Kamino, T., Yaguchi, T., Saka, H., 1995. TEM observation of micrometer-sized Ni powder particles thinned by FIB cutting technique. J. Electron Microsc. 44, 410–413.

Kitano, Y., Fujikawa, Y., Takeshita, H., Kamino, T., Yaguchi, T., Matsumoto, H., Koike, H., 1995. TEM observation of micrometer-sized Ni powder particles thinned by FIB cutting technique. J. Electron Microsc. 44, 376–383.

Krohn, V.E, 1961. Progress in Astronautics and Rocketry. Academic Press, New York pp. 73–90.

Lee, R.J., Morgan, J.C., 1991. Integration of a focused ion beam system in a failure analysis environment, Proceedings of the Seventeenth International Symposium for Testing and Failure Analysis, ISTFA '91, pp. 85–95.

Levi-Setti, R., Fox, T., Lam, K., 1983. Ion channeling effects in scanning ion microscopy with a 60 keV Ga + probe. Nucl. Instrum. Methods. 205, 299–309.

Levi-Setti, R., Crow, G., Wang, Y.L., 1985. Progress in high resolution scanning ion microscopy and secondary ion mass spectrometry imaging microanalysis. Scanning Electron Microsc. 11, 535–551.

Levi-Setti, R., Crow, G., Wang, Y.L., 1986. scanning ion microscopy: elemental maps at high lateral resolution. Applied Surface Sci. 26, 249–264.

Lo, J., Santos, R., Kuriakose, A.K., Carpenter, G., Lu, A., 1996. Squeeze casting silicon carbide particulate reinforced magnesium matrix composite. In: Hui, D. (Ed.), Proceedings of the Third International Conference on Composite Engineering, pp. 533–542.

Mallard, R.E., Clayton, R., Mayer, D., Hobbs, L., 1998. Failure analysis of high power GaAs-based lasers using electron beam induced current analysis and transmission electron microscopy. J. Vac. Sci. Technol. A 16 (2), 825–829.

McDermott, M., 1998. Head makers discover focused ion beams. Data Storage March, 23–26.

Melngailis, J., 1987. Critical review: focused ion beam technologies and applications. J. Vac. Sci. Technol. B 5 (2), 469–495.

Melngailis, J., 1993. Focused ion beam lithography. Nucl. Instrum. Methods. B 80/81, 1271–1280.

Melngailis, J., Musil, C.R., Stevens, E.H., Utlaut, M., Kellog, E.M., Post, R.T., Geis, M.W., Mountain, R.W., 1986. The focused ion beam and an integrated circuit restructuring tool. J. Vac. Sci. Technol. B 4, 176.

Milner, R., Phaneuf, M.W., 1998. Comparative carburization of heat resistant alloys. In: Corrosion 98, NACE International, Houston, in press.

Muroga, A., Saka, H., 1995. Analysis of rolling contact fatigued microstructure using focused ion beam sputtering and transmission electron microscopy observation. Scripta Metall. et Mater. 33, 151–156.

Nakagawa, Z., Sasaki, S., Sato, M., Glanville, J., Yamamoto, M., 1988. Summary Abstract: recent process on etching technology with focused ion beam in photomask repair. J. Vac. Sci. Technol. B 6 (3), 1030–1031.

Orloff, J., 1993. High-resolution focused ion beams. Rev. Sci. Instrum. 64 (5), 1105–1130.

Overwijk, M.H.F., van den Heuvel, F.C., 1993. Focused-ion-beam-induced tungsten deposition: theory and experiment. Nucl. Instrum. Methods. B 80/81, 1324–1327.

Overwijk, M.H.F., van den Heuvel, F.C., Bulle-Lieuwma, C.W.T., 1993. Novel scheme for the preparation of transmission electron microscopy specimens with a focused ion beam. J. Vac. Sci. Technol. B 11 (6), 2021–2024.

Park, K., 1990. Cross-sectional TEM specimen preparation of semiconductor devices by focused ion beam etching. In: Anderson, R. (Ed.), Materials Research Society Symposium Proceedings, MRS, Pittsburgh, 199, pp. 271–280.

Pease, R.F.W., Nixon, W.C., 1965. J. Phys. E. 42, 281.

Phaneuf, M.W., Rowlands, N., Carpenter, G.J.C., Sundaram, G., 1997. Focused ion beam sample preparation of non-semiconductor materials. In: Anderson, R. (ed.), Mat. Res. Soc. Symp., MRS, Pittsburgh, 480, pp. 39–48.

Phaneuf, M.W., 1998. Private communications with representatives of Micrion Corporation and FEI Corporation.

Presser, N., Hilton, M.R., 1997. Applications of focused ion beam machining to the characterization of carbide, nitride and oxide films. Thin Solid Films 308/309, 369–374.

Prewett, P.D., Mair, G.L.R., 1991. Focused ion beams from liquid metal ion sources, Research Studies Press Ltd., Taunton, Somerset, UK.

Prewett, P.D., 1993. Focused ion beams—microfabrication methods and applications. Vacuum 44 (3/4), 345–351.

Saitoh, K., Onoda, H., Morimoto, H., Katayama, T., Watakabe, Y., Kato, T., 1988. Practical results of photomask repair using focused ion beam technology. J.Vac. Sci. Technol. B 6 (3), 1032–1034.

Saka, H., Kato, T., Hong, M.K., Sasaki, K. and Kamino, T., 1995. Cross-sectional TEM observation of interfaces in a galvannealed steel, Galvatech '95: Proceedings of the Third International Conference on Zinc and Zinc Alloy Coated Steel Sheet, pp. 809–814.

Saka, H., Abe, S., 1997. FIB/HVEM observation of the configuration of cracks and the defect structure near the cracks. Jap. Soc. Electron Microsc. 1, 45–57.

Saka, H., Abe, S., 1997. Plan-view observation of crack tips by focused ion beam/transmission electron microscopy. Mat. Sci. Engng 234/236, 552–554.

Van Camp, R., Van Doorselaer, K., Clemminck, I., 1996. Reliability of a focused ion beam repair on digital CMOS circuits. Microelectron Reliab. 36, 1787–1790.

Wang, K., Garoche, P., Dumoulin, L., 1998. Focused ion beam imaging of grains in Al–Li–Cu quasicrystal. J. Phys.: Condens. Matter 10, 3479–3488.

Wang, Y.Z., Revie, W., Phaneuf, M.W., Li, J., 1999. Examination of stress corrosion crack profiles using focused ion beam microscopy. In: Analysis of In-Service Failures and Advances in Microstructural Characterization: Proceedings of the Thirtyfirst Conference of the International Metallographic Society (July 1998), American Society for Metals, Metals Park, OH. In press.

Young, R.J., Cleaver, J.R.A., Ahmed, H., 1993. Characteristics of gas-assisted focused ion beam etching. J. Vac. Sci. Technol. B 11 (2), 234–241.

Young, R.J., Kirk, E.C.G., Williams, D.A., Ahmed, H., 1990. Fabrication of planar and cross-sectional TEM specimens using a focused ion beam. In: Anderson, R. (ed.), Material Research Society Symposium Proceedings, MRS Pittsburgh, 199, pp. 205–216.

Young, R.J., 1993. Micro-machining using a focused ion beam. Vacuum. 44, 353–356.

Young, R.J., 1997. Application of the focused ion beam in materials characterization and failure analysis. Microstruct. Sci. 25, 491–496.